2nd URSI AT-RASC, Gran Canaria, 28 May–1 June 2018

Computation of Antenna Transfer Functions with a Bidirectional Ray-Tracing Algorithm Utilizing Antenna Reciprocity

Mehmet M. Taygur*, Ilya O. Sukharevsky, and Thomas F. Eibert
Technical University of Munich, Department of Electrical and Computer Engineering, Chair of High-Frequency Engineering, Munich, Germany

Abstract

A bidirectional ray-tracing algorithm based on the reciprocity theorem is introduced for calculating antenna transfer functions. Ray launching is carried out from both receiver and transmitter antennas. The transfer function is calculated by capturing the rays from both antennas on an interaction surface and by evaluating the reciprocity integral on this surface using a numerical integration technique. Reception spheres, which are utilized in the unidirectional Shooting and Bouncing Rays method, are replaced by the interaction surfaces as they are much more flexible in size and shape. Large geometries, which are cumbersome to simulate with traditional techniques, can be easily and accurately simulated in this way. Additionally, the interaction surfaces can be employed for the calculation of diffraction effects, instead of utilizing the Uniform Theory of Diffraction (UTD). Problems related to the branching in the ray tree can be avoided in this way.

1 Introduction

Ray-tracing is a widely utilized method for solving electrically large problems, such as the analysis of wireless communication links [1]. In general, a ray-tracing simulation consists of the calculation of the feasible ray paths between two points (i.e. a transmitting and a receiving antenna) and the calculation of the field expressions or the transfer function according to these ray paths. A common approach for the calculation of the ray paths is the Shooting and Bouncing Rays (SBR) where the rays are launched from the transmitter location in random directions. The feasible ray paths are obtained by capturing the rays at reception spheres. Uniform Theory of Diffraction (UTD) and the Geometrical Optics (GO) principles are usually adopted for the calculation of the fields [2].

SBR methods have limitations in terms of the number of ray launches and the size of the reception spheres. Specifically, either a large number of ray launches or large reception spheres are needed in order to simulate electrically large scenarios. However, the reception spheres may collect incorrect rays in the former case (leading to an inaccurate result) whereas the computation time may increase in the latter [3].

In this study, a novel ray-tracing algorithm, which is based on the reciprocity theorem and bidirectional ray-tracing, is introduced. The rays are launched not only from the transmitter, but from the receiver as well. The reception spheres do not exist as the rays are collected on an interaction surface, whose size and shape can be altered in contrast to a reception sphere. The antenna transfer function is calculated by evaluating the reciprocity integral on the interaction surface. The interaction surface can be also used to simulate wedge diffraction effects where the integration is performed on a surface restricted by an edge, in similar fashion as the Physical Optics (PO) approach. In this way, branching problems in the ray tree due to UTD can be avoided [4].

2 Reciprocity Theorem

Suppose that a receiver and a transmitter antenna, namely A and B, exist in the space and Ψ is a surface closed around A. Then, according to the reciprocity theorem, the electric and magnetic fields for A and B satisfy [5]

$$\oiint_{\Psi} [(\mathbf{H}_A \times \mathbf{E}_B) - (\mathbf{H}_B \times \mathbf{E}_A)] \cdot d\mathbf{S} = \iiint_{\Omega} [\mathbf{E}_B \cdot \mathbf{J}_A] \, dV, \tag{1}$$

where Ω is the volume which comprises A and which is bounded by Ψ. $\mathbf{J}_A$, $\mathbf{E}_A$, $\mathbf{H}_A$ and $\mathbf{J}_B$, $\mathbf{E}_B$, $\mathbf{H}_B$ are the impressed current densities at the terminals of the antennas, the electric fields and the magnetic fields for A and B, respectively. Eq. (1) can be further simplified as

$$\oiint_{\Psi} [(\mathbf{H}_A \times \mathbf{E}_B) - (\mathbf{H}_B \times \mathbf{E}_A)] \cdot d\mathbf{S} = V^{oc} I_A, \tag{2}$$

where V^{oc} is the induced open-circuit voltage at antenna A on receive and I_A is the port current of antenna A on transmit. Assuming that the generator voltage of B is known, the coupling between A and B is obtained by calculating the integral in (2). The computation of the coupling consists of four steps:

1. The rays coming from the receiver and transmitter sites are captured on the interaction surface.

2. The field expressions at the ray-surface intersections are calculated.

3. The field expressions are interpolated. Hence, the field is also known at the points which might be needed in the integration process but were not hit by the rays.

4. The integral is evaluated with an appropriate algorithm.

3 Oscillatory Integrals

The surface integral at the left-hand side of (2) consists of oscillatory phase terms, proportional to the wavelength λ. The evaluation of such an integral is extremely time consuming with traditional techniques, especially for large values of λ. Therefore, a special method suitable for an oscillatory integral is utilized. The integral in (2) can be expressed by

$$\oiint_{\Psi} [(\mathbf{H}_A(\mathbf{r}) \times \mathbf{E}_B(\mathbf{r})) - (\mathbf{H}_B(\mathbf{r}) \times \mathbf{E}_A(\mathbf{r}))] \cdot d\mathbf{S} = \oiint_{\Psi} f(\mathbf{r}) e^{jkg(\mathbf{r})} dS, \tag{3}$$

with

$$\Theta = [(\mathbf{H}_A(\mathbf{r}) \times \mathbf{E}_B(\mathbf{r})) - (\mathbf{H}_B(\mathbf{r}) \times \mathbf{E}_A(\mathbf{r}))] \cdot \hat{\mathbf{n}},$$
$$g(\mathbf{r}) = \frac{\arg(\Theta(\mathbf{r}))}{k}, \;\; f(\mathbf{r}) = ||\Theta|| \mathrm{sgn}\left(\Re\left(\frac{||\Theta|| e^{jkg(\mathbf{r})}}{\Theta} \right) \right), \tag{4}$$

where $f(\mathbf{r})$ is a magnitude function, $g(\mathbf{r})$ is a phase function, sgn(.) is the signum function, $\Re$ denotes the real part of a complex number, k is the propagation constant and $\hat{\mathbf{n}}$ is the surface normal vector. The integral is computed by applying linear approximations to f and g, then evaluating it analytically according to these linear functions. Since the approximation may be inaccurate for the entire integration domain, it is useful to subdivide the domain and calculate the integrals on these sub-domains individually. A practical technique for the subdivision is triangulation [6]. Thus, the sub-domains have triangular shapes. Then, the integral can be written as

$$\oiint_{\Psi} f(\mathbf{r}) e^{jkg(\mathbf{r})} dS \approx \sum_{t=1}^{T} \left(\iint_{\Psi_t} \tilde{f}_t(\mathbf{r}) e^{jk\tilde{g}_t(\mathbf{r})} dS \right), \tag{5}$$

where T is the number of the triangles in Ψ, Ψ_t denotes the triangle t, $\tilde{f}_t$ and $\tilde{g}_t$ are the linear approximations of f and g in t, respectively. The accuracy of the integration is strongly dependent on the accuracy of the linear approximation in each sub-domain.

4 Constructing the Field Expressions

The integration process described in [6] imposes the field expressions to be found at each corner of each triangle. Therefore, it is necessary to perform interpolation since the incoming rays usually do not hit the corners. For a given triangle t and an arbitrary point $\mathbf{P} \in t$, the procedure to obtain the field expressions at $\mathbf{P}$ can be summarized as follows:

1. Let us assume that n rays from the same wavefront intersect with the triangle t and the intersection points are defined by $\mathbf{C}_{1,\cdots,n}$. It is assumed that all the information regarding the wavefront is known at these points. The propagation phase information is obtained by the ray path length difference between $\mathbf{P}$ and any one of the intersection points ($\mathbf{C}_{1,\cdots,n}$).

2. Let the rays which cross $\mathbf{C}_{1,\cdots,n}$ have propagation directions $\mathbf{D}_{1,\cdots,n}$. The polarization and amplitude of the field at $\mathbf{P}$ are obtained from the field information at $\mathbf{C}_{1,\cdots,n}$ by interpolation with respect to $\mathbf{D}_{1,\cdots,n}$.

3. The polarization, phase and amplitude information calculated in the previous steps are utilized to obtain the field at point $\mathbf{P}$.

The number of the rays needed for the interpolation of each wavefront is 5 in our problems ($n = 5$). The process is repeated for each triangle corner.

5 Bidirectional Ray-Tracing with GPU Computing

Graphics Processing Unit (GPU) based computing has recently emerged as a useful method for electromagnetic ray-tracing simulations. Due to the similarities between the ray-tracing concepts for computer graphics and electromagnetics, the GPU computing tools which were originally designed for computer graphics applications, can be employed for solving electromagnetic problems as well [7]. The ray-tracing software, which has been used in this study, is based on Thrust Standard Template Library and OptiX™ ray-tracing engine from NVIDIA [8].

5.1 Bidirectional Ray-Tracing

The bidirectional ray-tracing is based on launching rays simultaneously from the source and the observer sites. These rays are usually captured and merged on an object for computing the transfer function [9, 10]. In this study, an interaction surface has been used for capturing and merging. The interaction surface is a transparent object which only collects the field information. It does not alter the rays or the fields in any way. Individual launches from the receiver and the transmitter are handled according to the unidirectional ray-tracing principles. The code can be divided into three parts, which are presented with brief explanations below:

1. *Geometry and Configuration Processor*: The geometry and simulation configuration information, such as the mesh data, material properties, antenna patterns,

number of ray launches, are processed. This section is executed on the CPU.

2. *Ray-Tracer*: The relevant ray paths between the antennas and the interaction surface are calculated. The algorithm is based on NVIDIA OptiX™, which identifies ray-object interactions automatically. The rays, which hit the interaction surface at least once, are saved. The ray-tracer also provides an alias ray elimination module where some of the rays having the identical ray path histories are eliminated.

3. *Postprocessor*: The postprocessor handles the calculation of the electromagnetic fields associated with the rays. The calculations are performed according to the interaction information (e.g. reflection, diffraction) extracted from the ray history. At the end of the process, all the necessary information would be obtained for evaluating the reciprocity integral on the interaction surface.

6 Numerical Results

The performance of the proposed method has been evaluated in two different scenarios. The results have been compared with unidirectional ray-tracing simulations as the path gain between a transmitter and a receiver is calculated. One bidirectional ray-tracing and two unidirectional ray-tracing simulations have been performed in total. The first unidirectional ray-tracing simulation has been executed with the same number of ray launches as in the bidirectional ray-tracing whereas the second one involves a larger number of ray launches to ensure the convergence of the result. The latter unidirectional ray-tracing simulation is also used as a reference for the other two simulations.

The operating frequency was chosen as 2 GHz. Half-wavelength dipole patterns were assumed for both transmitter and receiver. In the unidirectional ray-tracing simulations, the radius of the reception spheres was chosen as 1λ.

6.1 Two-Ray Ground Reflection Scenario

The receiver and the transmitter are located 5 m above a metallic ground plane. The distance between the antennas varies from 5 m to 20 m with 5 m steps. For the bidirectional ray-tracing simulation, a cube, whose side length is 8 m, is placed around the receiver and acts as the interaction surface. The illustration of the scenario is shown in Fig. 1 and the results are given in Fig. 2.

The results show that the bidirectional ray-tracing is more accurate than the unidirectional ray-tracing simulation under the same circumstances, i.e. equal number of ray launches, when the problem geometry is large. It can be

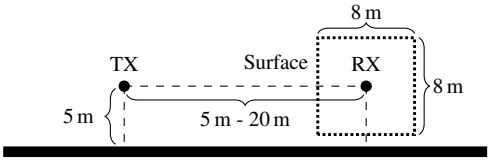

Figure 1. Illustration of two-ray ground reflection scenario.

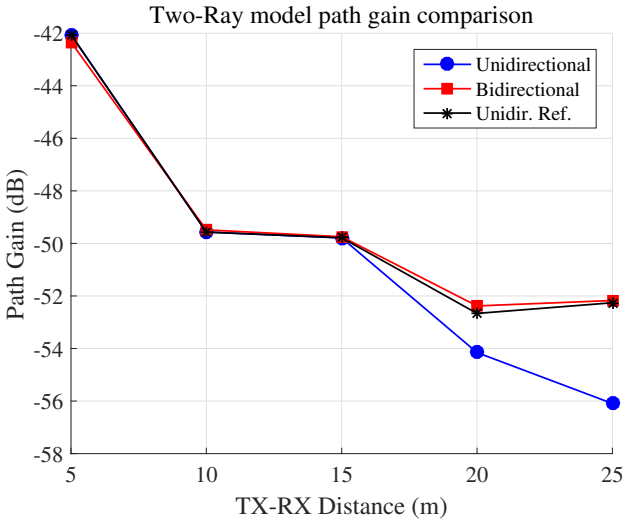

Figure 2. Two-Ray model path gain comparison.

observed that the path gain value for the unidirectional ray-tracing deviates from the reference when the antenna distance is beyond 15 m, since the algorithm cannot determine all the correct ray paths.

6.2 Simulation of Diffraction Effects with an Open Interaction Surface

A half-plane edge diffraction geometry is created where the receiver and transmitter antennas are in the shadow regions, thus, the edge diffraction is the only coupling mechanism. In this scenario, the unidirectional ray-tracing method requires UTD computations whereas the bidirectional ray-tracing algorithm works with the rays which are incident upon a large, open interaction surface located above the edge. The coupling is determined by evaluating the reciprocity integral on this surface using the incident rays. Hence, the computation of the path gain is carried out with a PO-like method, which is different than UTD and eliminates the issues regarding the branching in the ray tree.

The scenario includes 1 transmitter and 4 receivers, all of which are located 5 m below the tip of the edge. The transmitter is 10 m away from the plane and the receivers are placed with 5 m, 10 m, 15 m and 20 m distance away from the plane, at the opposite side. The interaction surface is located above the edge and it reaches 80 m height. An illustration of the problem geometry is shown in Fig. 3 and the results are given in Fig. 4.

Similar to the previous scenario, the unidirectional ray-

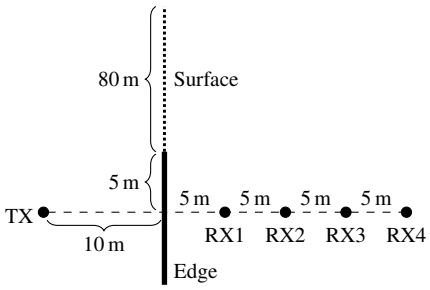

Figure 3. Simulating single edge diffraction with an interaction surface.

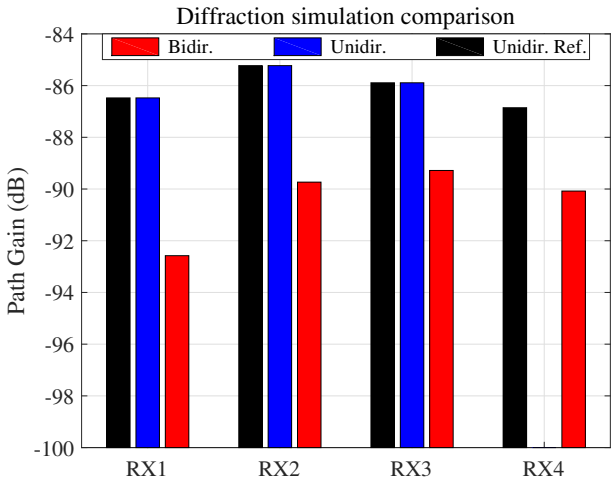

Figure 4. Half-plane diffraction path gain comparison.

tracing fails to find the ray path when the distance between the transmitter and the receiver is large. On the other hand, the bidirectional ray-tracing method can provide good results even when the unidirectional ray-tracing fails. The results indicate that the bidirectional ray-tracing algorithm achieves a better accuracy when the antennas are closer to the optical boundaries (RX4) where the deviation is only 3 dB. The observed deviations are similar to what is expected as difference between PO and UTD results.

7 Conclusion

A novel bidirectional ray-tracing technique, which uses the reciprocity theorem for computing the antenna transfer function, has been introduced. The transfer function is obtained by computing the reciprocity integral on interaction surfaces, which eliminates the need for the reception spheres. The new method avoids the shortcomings of the reception spheres in large geometries. Furthermore, the method has been utilized in a half-plane diffraction scenario where the diffraction effect is simulated by a PO-like integration instead of UTD. Thus, the computational costs of UTD regarding the ray branching are avoided.

Acknowledgements

Ilya O. Sukharevsky is supported by the Alexander von Humboldt Foundation.

References

[1] M. Iskander and Z. Yun, "Propagation Prediction Models for Wireless Communication Systems," *IEEE Transactions on Microwave Theory and Techniques*, **37**, 2, March 2002, pp. 662-673.

[2] Z. Yun and M. Iskander, "Ray Tracing for Radio Propagation Modeling: Principles and Applications," *IEEE Access*, **3**, 2015, pp. 1089-1100

[3] S. Seidel and T. Rappaport, "Site-Specific Propagation Prediction for Wireless In-Building Personal Communication System Design," *IEEE Transactions on Vehicular Technology*, **43**, 4, November 1994, pp. 879-891.

[4] R. Kouyoumjian and P. Pathak, "A uniform geometrical theory of diffraction for an edge in a perfectly conducting surface," *Proceedings of the IEEE*, **62**, 11, 1974, pp. 1448-1461.

[5] R. Collin and F. Zucker, *Antenna Theory*, McGraw-Hill, 1989.

[6] O. Sukharevsky, *Electromagnetic Wave Scattering by Aerial and Ground Radar Objects*, CRC Press Inc., 2014.

[7] M. Mocker, M. Schiller, R. Brem, Z. Sun, H. Tazi, T. Eibert, and A. Knoll, "Combination of a Full-Wave Method and Ray Tracing for Radiation Pattern Simulations of Antennas on Vehicle Roofs," 9th European Conference on Antennas and Propagation (EUCAP), Lisbon, Portugal, August 2015, pp. 1-5.

[8]] S. Parker et al., "Optix: A General Purpose Ray Tracing Engine," *ACM Transactions on Graphics*, **29**, 4, July 2010, pp. 1-13.

[9] F. Xu and Y.-Q. Jin, "Bidirectional Analytic Ray Tracing for Fast Computation of Composite Scattering from Electric-Large Target Over a Randomly Rough surface," *IEEE Transactions on Antennas and Propagation*, **57**, 5, 2009, pp. 1495-1505

[10] E. Lafortune and Y. Willems, "Bi-directional path tracing," International Conference on Computational Graphics and Visualization Techniques, Algarve, Portugal, December 1993, pp. 145-153.